Soft Matter

Refractive-index and density-matched emulsions with programmable DNA interactions

Journal:	*Soft Matter*
Manuscript ID	SM-ART-01-2024-000032.R1
Article Type:	Paper
Date Submitted by the Author:	01-Mar-2024
Complete List of Authors:	Chen, Wenjun; New York University Graduate School of Arts and Science, Department of Physics Sixdenier, Lucas; New York University McMullen, Angus; New York University, Grier, David; New York University, Department of Physics Brujic, Jasna; New York University, Department of Physics

Soft Matter

ARTICLE TYPE

Cite this: DOI: 00.0000/xxxxxxxxxx

Refractive-index and density-matched emulsions with programmable DNA interactions

Wenjun Chen, Lucas Sixdenier, Angus McMullen, David G. Grier, and Jasna Brujic*

Received Date
Accepted Date

DOI: 00.0000/xxxxxxxxxx

Emulsion droplets on the colloidal length scale are a model system of frictionless compliant spheres. Direct imaging studies of the microscopic structure and dynamics of emulsions offer valuable insights into fundamental processes, such as gelation, jamming, and self-assembly. A microscope, however, can only resolve the individual droplets in a densely packed emulsion if the droplets are closely index-matched to their fluid medium. Mitigating perturbations due to gravity additionally requires the droplets to be density-matched to the medium. Creating droplets that are simultaneously index-matched and density-matched has been a long-standing challenge for the soft-matter community. The present study introduces a method for synthesizing monodisperse micrometer-sized siloxane droplets whose density and refractive index can be precisely and independently tuned by adjusting the volume fraction of three silane precursors. A systematic optimization protocol yields fluorescently labeled ternary droplets whose densities and refractive indexes match, to the fourth decimal place, those of aqueous solutions of glycerol or dimethylsiloxane. Because all of the materials in this system are biocompatible, we functionalize the droplets with DNA strands to endow them with programmed inter-droplet interactions. Confocal microscopy then reveals both the three-dimensional structure and the network of droplet-droplet contacts in a class of self-assembled droplet gels, free from gravitational effects. This experimental toolbox creates opportunities for studying the microscopic mechanisms that govern viscoelastic properties and self-assembly in soft materials.

1 Introduction

Colloidal dispersions are valuable model systems for experimental studies of many-body phenomena. The individual particles are small enough to explore complex phase spaces under the influence of random thermal forces yet large enough to observe in real space through conventional light microscopy[1–6]. Multiple light scattering obscures the dynamics of individual particles in the bulk of dense three-dimensional dispersions unless care is taken to match the particles' refractive index to that of the fluid medium. Studies on index-matched dispersions have revealed the microscopic origin of a range of phenomena, including the mechanisms of three-dimensional melting and freezing[7–9], gelation[10,11], jamming[12], and the glass transition[13,14]. Gravity influences the behavior of micrometer-scale colloidal particles and imposes uniaxial stress that can qualitatively alter their collective behavior[11,15–23]. Previous experimental studies have mitigated the influence of gravity either by density-matching the particles using solvent mixtures[24–34] or else by transporting the system to a microgravity environment[16,21,23,35]. Nearly all of these prior studies focus on the behavior of solid particles that interact through hard-sphere repulsions in the normal direction and frictional forces tangentially. Compliance[36] and friction[37] are both believed to be singular perturbations for processes such as jamming and freezing. These considerations highlight the desirability of emulsion droplets as compliant and inherently frictionless model particles, whose inter-particle interactions are tunable via surface chemistry, and whose refractive index and density can be simultaneously matched to the medium.

Lipid-stabilized emulsion droplets constitute an experimentally accessible model for soft frictionless spheres[38–41]. The incompressible droplets deform elastically under compression or extension[40]. Their liquid interfaces allow them to slip and rotate freely when they come into contact, effectively eliminating friction[38,39,41]. The lipid surfactant, furthermore, can be functionalized to implement specific interparticle interactions, giving rise to attractive gels with unique mechanical and packing properties, as predicted by both theory and numerical simulations[4,42–48].

Here we introduce a novel synthetic protocol for lipid-stabilized emulsions that yields stable, monodisperse droplets whose density and refractive index are simultaneously matched to an aqueous solution that is biocompatible and nontoxic. This contrasts with a previously reported protocol for matched emulsions[49] that yields polydisperse droplets dispersed in a solution containing for-

* Center for Soft Matter Research and Department of Physics, New York University, New York, New York, 10003, USA. E-mail: jb2929@nyu.edu

mamide, which is both toxic and volatile. The single-pot synthesis is inherently scalable. Droplets can be optimized for diameters ranging from 1 μm to 10 μm and can be matched for both refractive index and density with an accuracy of 100 parts per million. These emulsions are robust against centrifugation and remain neutrally buoyant over several days. Concentrated emulsions have an optical penetration depth of several millimeters. Completed droplets can be can be fluorescently labeled and specifically functionalized, as shown in Fig. 1. Split-and-mix processing[50] then can be used to create multifunctional monodisperse emulsions that self-organize into preprogrammed sequences and hierarchically ordered structures.

With these tools in hand, we use confocal microscopy to map the distribution of particles in concentrated 3D emulsions under conditions of positive, negative, and neutral buoyancy. We then use the biocompatibility of the aqueous phase to functionalize the droplets with lipids that carry selected sequences of single-stranded DNA. These DNA sticky ends implement a programmed matrix of inter-droplet interactions[40,51] that is validated through confocal imaging of droplet contacts within 3D packings. Imaging also verifies the planned valence of the droplet contact network and the flexibility of the DNA-mediated droplet-droplet bonds[39–41,52,53].

2 Experimental Section

2.1 Materials

For droplet synthesis, diethoxydimethylsilane (DMDES, 98 percent), ammonia (27 vol% aqueous solution), sodium dodecyl sulfate ($\geq$ 99.0 %), dimethylsulfoxide (DMSO, $\geq$ 99.9 %), and glycerol are purchased from Sigma-Aldrich. The dye 4,4-difluoro-1,3,5,7,8-pentamethyl-4-bora-3a,4a-diaza-s-indacene (BODIPY 493/503, 99 %) is purchased from Thermo Fisher Scientific. Two other silanes, phenylmethyldiethoxysilane (PMDES, 97 %) and (3,3,3-trifluoropropyl) methydimethoxysilane (TFPMDMS, 97 %) are purchased from Gelest. All solutions are prepared using deionized water with 18.2 M■cm resistivity, obtained from a Millipore Filtration System (Milli-Q Gradient A10). BODIPY solution is prepared at 1 mg/mL in ethanol.

2.2 Droplet synthesis protocol

The single-pot preparation of monodisperse matched emulsions is illustrated in Fig. 2. We present the protocol in the context of preparing a typical 1.5 mL sample of monodisperse emulsion. These droplets are created using 5 vol% monomers and 5 vol% ammonia.

2.2.1 Prehydrolysis

To prepare 1.5 mL of 5 vol% droplet emulsion, monomers are first hydrolyzed by adding 75 μL of monomers to 1335 μL of deionized water in a 2 mL glass vial and then stirring the solution in a vortex mixer (Vortex-Genie 2) at 2500 rpm for up to 5 min and thereafter on a shaker (IKA minishaker MS 3 basic) at 1000 rpm for at least 6 h to vigorously homogenize the mixture. The time required to complete the prehydrolysis varies with the amount and type of silane monomers used. PMDES and TFPMDMS hydrolyze more slowly than DMDES; a 5 vol% mixture typically requires 12 h to completely dissolve. If the monomers are still not completely dissolved after 12 h, the solution can be further stirred in a vortex mixer for 5 min and tumbled on a shaker for another 6 h to obtain a uniformly transparent solution.

2.2.2 Emulsification

After prehydrolysis, 75 μL of ammonia (27 vol% solution) is added to catalyze droplet nucleation. The solution is mixed by gently tumbling the glass vial, taking care to avoid overly vigorous mixing that could increase polydispersity. The solution then is left on the rotator for 24 h to allow droplets to grow. Once the sample is taken off the rotator, 15 μL of 100 mM SDS solution is added to the sample with continued gentle tumbling to reach a final SDS concentration of 1 mM.

The completed droplets are washed with 1 mM SDS solution three times to stop further growth and are stored in a 5 mM SDS solution. Figure 3(a) presents a bright-field micrograph of a typical sample of monodisperse emulsion droplets. Because these droplets are neither density matched nor index matched to the aqueous medium at this point, they sediment into a monolayer that can be imaged directly.

To prepare a 100 mL droplet dispersion made using 5 vol% monomers and 5 vol% ammonia, we first add 5 mL of monomers to 89 mL of deionized water in a 250 mL glass Erlenmeyer flask. The mixture is vigorously stirred using a magnetic stirrer (IKA 3671000 Color Squid White Magnetic Stirrer) at 800 rpm for at least 6 h to obtain a homogeneous solution. We then reduce the stirring speed to 100 rpm and add 5 mL of ammonia to the sample. The sample is left on the stirrer to grow for 24 h. Once the droplets have grown to their final size, 1 mL of 100 mM SDS solution is added to reach a final SDS concentration of 1 mM. The droplets are then washed three times with a 1 mM SDS solution by centrifugation or dialyzed against a 1 mM SDS solution to prevent further growth. The completed dispersion is stored in a 5 mM SDS solution until further use.

2.3 DNA functionalization

Single-stranded DNA is purchased from Integrated DNA Technologies with sequences reported in Table 1. Linker strands, L and L′, have 20 complementary base pairs (bps) at their 3′ end (sticky ends). The P strand has a self-complementary palindrome sequence of 6 bps at its 3′ end. The complementary spacer (CS) strand is complementary to the 50 first bps that are common to L, L′, and P. An azide group is added at the end of each strand (5′ end for L and L′, and 3′ end for CS) to facilitate coupling the strands to lipid surfactants via click chemistry.

Droplets are functionalized with lipid-tethered DNA strands according to a protocol adapted from Refs. 39–41. Briefly, each sticky DNA strand (L, L′, P) and the complementary spacer strand (CS) are coupled to a DBCO-terminated pegylated lipid (DSPE-PEG(2000)-DBCO, Avanti Polar Lipids) via an azide-alkyne click reaction, before being annealed from 70 °C to room temperature. The resulting lipid-tethered double-stranded DNA duplex is stored at 10 μM in a buffer containing 10 mM Tris, 1 mM EDTA, and 50 mM NaCl (buffer A).

Droplets are functionalized by incubating 5 vol% of packed droplets with 100 nM of the appropriate DNA duplex in buffer A for 30 min. The functionalized droplets are stabilized by adding 0.1 wt% of Pluronic F68. Then, the droplets are washed through two cycles of centrifugation, supernatant removal, and redispersion, once in buffer A supplemented with 0.1 wt% of Triton X165, and once in pure buffer A, respectively. The droplets are finally redispersed at 5 vol% in buffer A.

2.4 Characterization

2.4.1 Droplet diameter

The size distribution of the droplets is measured by Total Holographic Characterization[54,55] with xSight (Spheryx, Inc.). The measurements are made at 23 °C at a vacuum wavelength of 450 nm. A 30 μL aliquot of droplet emulsion is pipetted into the sample reservoir of an xCell8 microfluidic chip (Spheryx, Inc.), which is mounted in xSight. The automated measurement process transfers 6 μL of the sample through the channel, recording and analyzing holograms of several thousand droplets. This analysis yields each droplet's diameter with a precision of ± 2 nm[56]. The polydispersity index for the sample is calculated as the standard deviation divided by the mean particle diameter. Typical results are plotted in Fig. 3(b).

2.4.2 Droplet refractive index

Total Holographic Characterization with xSight also yields the refractive index of each droplet with a precision of $\Delta n = \pm 5 \times 10^{-4}$ [54,56]. Measurements performed at vacuum wavelengths of 640 nm, 520 nm and 450 nm can be combined to estimate the dispersion of the droplets' refractive index.

The holographically measured droplet refractive index is validated by coalescing the droplets into a continuous phase whose refractive index is measured with an Abbe refractometer (Atago NAR-3 T). Droplets are coalesced by adding $CaCl_2$ to reach a final concentration of 10 mM and then stirring in a vortex mixer. The refractive index is then measured at a vacuum wavelength of 589 nm at 23 °C.

Refractive index measurements are used to map the ternary composition space for the three-component droplets, as shown in Fig. 4(a), and to traverse that space to achieve desired properties, as shown in Fig. 4(b).

2.4.3 Droplet density

To estimate the droplet density, we measure the total dispersion density at four different droplet mass fractions and then extrapolate to 100 % droplet mass fraction. An Anton-Paar DMA 4500 M density meter is used to measure the densities of the droplet dispersions. All density measurements are performed at 23 °C.

To determine the mass fraction of droplets in dispersion, we weigh the dispersion before and after drying it in a vacuum desiccator (Bel-Art) with desiccants (Drierite^{TM} Drying Desiccants, W.A. Hammond). Drying removes the aqueous phase, but not the silanes.

2.4.4 Index matching

The transparency of the emulsion is evaluated by measuring the optical transmittance of a 5 mL sample in the visible range using a UV-Vis spectrometer (Agilent Cary 3500 UV-vis Spectrometer). Transparency is maximized when the refractive index of the droplets matches that of the continuous aqueous phase. Typical results are presented in Fig. 5.

2.4.5 Density matching

The buoyant density of the droplets is measured by placing samples dyed with BODIPY in a 0.1 mm × 1 mm rectangular capillary (Vitrocom) and imaging the droplets on a Leica SP8 confocal microscope equipped with a Leica glycerol immersion objective lens (HCX PL APO 63×/1.3 GLYC CORR CS (21 °C)). Z-stacks are acquired in reflection mode with a continuous-wave 488 nm (cyan) laser. Positions of the individual droplets are obtained from these raw data using the TrackMate package[57] in the Fiji image analysis platform[58] and are analyzed to estimate the density mismatch between the droplets and the aqueous medium.

The mass density difference, $\Delta\rho$, between the droplets and the surrounding medium is estimated from the measured velocity of the droplets, v, using the formula

$$\Delta\rho = 18\frac{\eta v}{d^2 g}, \quad (1)$$

where η is the dynamic viscosity of the medium, d is the mean droplet diameter, and $g = 9.81\,\mathrm{m/s^2}$ is the acceleration due to gravity. For a 42 wt% glycerol solution at 23 °C, $\eta = 3$ cP.

Density-matched droplets remain suspended in the 100 μm-deep channel without sedimenting for a week, implying that $v \ll 0.2\,\mathrm{nm/s}$. For the matched droplets shown in Fig. 5, which have a diameter of $d = 1.5\,\mu$m, this means that $\Delta\rho \ll 5 \times 10^{-4}\,\mathrm{g/cm^3}$.

3 Results and Discussion

3.1 Droplet synthesis

To synthesize polysiloxane oil droplets, we implement the protocol depicted in Fig. 2(a), using the formation of polydimethysiloxane (PDMS) droplets as an example. This protocol is adapted from Refs. 59–61, as outlined in Refs. 39–41,53. The synthesis starts with the prehydrolysis of alkoxysilane monomers (here dimethoxydiethylsilane, DMDES) in water. Ammonia is added to the solution to catalyze the condensation of the hydrolyzed silane units into hydrophobic siloxane oligomers (here PDMS chains) that spontaneously form droplet nuclei upon phase separation. The nuclei then are left to grow into droplets of desired sizes by progressively incorporating additional silane units. Ultimately, sodium dodecyl sulfate (SDS) surfactant is added to stabilize the droplet interfaces, resulting in monodisperse suspensions of micrometre-sized droplets (Fig. 3(a)).

Among the parameters that govern droplet size, the most important are the volume fractions of monomer and ammonia. More specifically, increasing the volume fraction of monomers or decreasing that of ammonia leads to the formation of increasingly large droplets, as shown in Fig. 3(c). This is because the amount of ammonia directly determines the number of nuclei formed, while free hydrolyzed DMDES monomers dictate the availability

of silane units that can be incorporated into the droplets. In other words, a scarcity of nuclei and an abundance of monomers results in larger droplets.

To vary the refractive index and density of the emulsion, we prepare droplets using three types of monomers: DMDES, phenylmethyldiethoxysilane (PMDES) and (3,3,3-trifluoropropyl)methydimethoxysilane (TFPMDMS) (See Fig. 2(b)). These monomers have similar structures, notably two alkoxysilane functions that are involved in the formation of the oligomer backbone, but they differ in their alkyl side groups. Accordingly, the densities of DMDES, TFPMDMS, and PMDES are 0.865 g/cm^3, 1.089 g/cm^3 and 0.963 g/cm^3, and their refractive indices are 1.380, 1.358, and 1.469, respectively. By varying the ratios of volume fractions of the three types of monomers, we produce droplets with a range of densities from 0.88 g/cm^3 to 1.28 g/cm^3, and refractive indices from 1.38 to 1.55, as shown in Fig. 4(a).

3.2 Index matching and density matching

To match both the refractive index and the density of the droplets, we prepare aqueous mixtures of either DMSO or glycerol in 1 mM SDS. From Fig. 4(b), we identify by interpolation the formulations that achieve matching for both parameters. For example, droplets synthesized using a binary mixture of 68.5 % DMDES and 31.5 % TFPMDMS (refractive index 1.3861) match with an aqueous solution containing 41.6 wt% of glycerol. Alternatively, droplets of 81.3 % DMDES and 18.7 % TFPMDMS can be matched with 35.9 vol% DMSO solution.

The UV-Vis transmittance spectrum plotted in Fig. 5(a) shows that optimally formulated droplets are index-matched to their buffer across the entire visible spectrum. Even at a density of 7 vol%, the dispersion is essentially transparent, which is confirmed by visual inspection in Fig. 5(b). The same droplets form an opaque dispersion when they are dispersed in pure water at the same concentration, and even when they are diluted a hundred-fold.

To check how well the transparent droplets are density matched, we label them with a fluorescent dye (1 vol% of BODIPY solution) for imaging with confocal microscopy. Figure 5(c) shows the integrated fluorescence intensity in vertical slices through two emulsions after five days of equilibration. The optimally formulated emulsion shows no trend along the vertical axis, which is consistent with the uniform distribution of droplets in the confocal image in Fig. 5(d). The absence of a trend is consistent with successful density matching down to at least the fourth decimal place, given the droplet size. Deliberately mismatching the density by $\Delta\rho = 0.007\,\mathrm{g/cm^3}$ with a composition of 70.0 % DMDES and 30.0 % TFPMDMS yields clear evidence of creaming on the same time scale, as shown by the nonuniform fluorescence yield from top to bottom in Fig. 5(c, red data). This also is consistent with the vertical confocal slice in presented in Fig. 5(e) for the mismatched droplets.

To test the sensitivity of our system, we synthesize larger droplets with a diameter of 3.5 μm and a refractive index of 1.3850, using 1 vol% of ammonia and 5 vol% of monomers (73.4 % DMDES, 26.6 % TFPMDMS). We achieve simultaneous matching in refractive index and density using an aqueous phase containing 40.6 wt% of glycerol and 5 mM SDS (see Fig. 6(b)). A tiny variation (0.5 wt%) of the glycerol content causes the droplets to either sink or cream, as shown in Fig. 6(a) and 6(c), respectively. Here, the difference between the densities of the matching aqueous phases measured in Fig. 6(b) corresponds to density matching better than 0.001 g/cm^3. We can vary the weight fraction of glycerol by 0.1 wt%, matching densities to within 10^{-4} g/cm^3.

3.3 Functionalization of droplets with DNA

Because the aqueous phase is biocompatible, the matched emulsion is amenable to functionalization with biological molecules, such as DNA or proteins[62]. Here we show that a lipid-DNA conjugated complex is adsorbed onto the droplet surface, as illustrated in Fig. 1, without significantly changing the refractive index. Droplets are synthesized using 0.2 vol% of ammonia and 5 vol% of monomers (74.0 % DMDES, 26.0 % TFPMDMS), yielding a sample with a mean diameter of 6 μm and a refractive index of 1.3850. To accommodate the stickiness of DNA and to stabilize the emulsion, the glycerol-containing aqueous phase is supplemented with 5 mM Tris, 5 mM $MgCl_2$ and 0.05 wt% F68 surfactant, which changes its density. Consequently, the amount of glycerol is adjusted to 40.3 wt% to maintain density matching.

The droplets are functionalized with single-stranded DNA sequences (labeled with blue fluorophores), whose complementary strands coat a second emulsion (labeled with yellow fluorophores), causing the droplets to bind through DNA hybridization. The two types of droplets are mixed together (at $\sim 1:1$ volume ratio) to give a uniform three-dimensional dispersion of bound droplets (Fig. 7(a)). When viewed at the scale of individual droplets (Fig. 7(b)), the presence of a droplet-droplet bond is revealed by the formation of a patch with enhanced fluorescence at the contact point. This signature results from the colocalization and hybridization of complementary DNA strands[39,40,63]. In contrast, non-contacting droplets on sub-resolution lengthscales do not exhibit such enhancement (Fig. 7(b)). The ability to identify and study adhesion between droplets in three dimensions in the absence of gravity opens the experimental platform for the design and development of new colloidal architectures.

The specific interactions mediated by complementary DNA linkers favor the formation of dimers and trimers of droplets. To increase the connectivity between the droplets, we also incorporate palindromic DNA strands that promote non-specific binding among all droplets. The addition of palindrome interactions increases the adhesive strength of bonds between droplets and leads to the formation of highly interconnected three-dimensional droplet networks, as shown in Fig. 7(c). Each droplet in this network displays multiple adhesion patches. The possibility to produce high-valence assemblies of density-matched droplets paves the way to the study of gelation in three dimensions and to the design of programmable bio-inspired materials. Image reconstruction of the particle centers and the areas of deformation between contacting droplets can be used to estimate inter-droplet forces

relative to the single-droplet surface tension[51,64,65]. The map of the structural network then can be used to determine the force moment tensor at the particle scale and the full stress tensor at the system scale[48]. This experimental platform therefore enables comprehensive comparison at the single particle scale between experiments, numerical simulations, and theory, which will be undertaken for our system in the future.

4 Summary and Conclusions

We present a preparatory protocol for highly monodisperse emulsion droplets whose refractive index and density can be simultaneously matched to the aqueous phase. Monodisperse matched emulsions offer several advantages over previously reported model colloidal systems. Emulsion droplets act as frictionless, deformable particles whose interactions can be precisely tuned. Precise density matching eliminates the influence of gravity on collective phenomena such as gelation, jamming and crystallization[16,30,66], which can now be revisited. Another exciting avenue of research is the study of mixing suspension flows in the absence of friction[67–70], which is a notable industrial challenge. Moreover, the biocompatibility of our system paves the way for biomimicry, including the study of the influence of DNA-mediated adhesion and assembly on the emulsion architecture. Furthermore, recent progress in folding colloidal polymers in 2D[41] will be extended into 3D to make colloidal protein analogs. In addition to their fundamental interest, folded colloidal polymers will serve as building blocks for novel functional materials[71,72].

Conflicts of interest

There are no conflicts to declare.

Acknowledgements

We would like to acknowledge Rodrigo E. Guerra for his insightful comments and we thank Lauren E. Altman and Rushna Quddus for their help with experiments. L.S., A.M., and J.B. were supported by the National Science Foundation under grant number NSF DMR-2105255. D.G.G. was supported by the NSF under award number DMR-2104837. The Spheryx xSight used for this study was acquired as shared instrumentation with support from the MRSEC program of the NSF under award number DMR-1420073.

References

1 C. A. Murray and D. G. Grier, Annu. Rev. Phys. Chem., 1996, **47**, 421–462.
2 A. D. Dinsmore, J. C. Crocker and A. G. Yodh, Curr. Opin. Colloid Interface Sci., 1998, **3**, 5–11.
3 A. Yethiraj, Soft Matter, 2007, **3**, 1099–1115.
4 M. van Hecke, J. Phys. Condens. Matter, 2009, **22**, 033101.
5 P. J. Lu and D. A. Weitz, Annu. Rev. Condens. Matter Phys., 2013, **4**, 217–233.
6 B. Li, D. Zhou and Y. Han, Nat. Rev. Mater., 2016, **1**, 1–13.
7 P. N. Pusey and W. Van Megen, Nature, 1986, **320**, 340–342.
8 P. Bartlett, R. Ottewill and P. Pusey, J. Chem. Phys., 1990, **93**, 1299–1312.
9 T. Palberg, J. Phys. Condens. Matter, 2014, **26**, 333101.
10 M. M. van Schooneveld, V. W. de Villeneuve, R. P. A. Dullens, D. G. Aarts, M. E. Leunissen and W. K. Kegel, J. Phys. Chem. B, 2009, **113**, 4560–4564.
11 D. Bonn, J. Otwinowski, S. Sacanna, H. Guo, G. Wegdam and P. Schall, Phys. Rev. Lett., 2009, **103**, 156101.
12 A. I. Campbell and M. D. Haw, Soft Matter, 2010, **6**, 4688–4693.
13 K. Jensen, D. A. Weitz and F. Spaepen, Phys. Rev. E, 2014, **90**, 042305.
14 E. R. Weeks, ACS Macro Lett., 2017, **6**, 27–34.
15 J. Bibette, T. Mason, H. Gang and D. Weitz, Phys. Rev. Lett., 1992, **69**, 981.
16 Z. Cheng, P. Chaikin, J. Zhu, W. Russel and W. Meyer, Phys. Rev. Lett., 2001, **88**, 015501.
17 S. Manley, L. Cipelletti, V. Trappe, A. Bailey, R. J. Christianson, U. Gasser, V. Prasad, P. Segre, M. Doherty, S. Sankaran et al., Phys. Rev. Lett., 2004, **93**, 108302.
18 S. Manley, J. Skotheim, L. Mahadevan and D. A. Weitz, Phys. Rev. Lett., 2005, **94**, 218302.
19 H. Guo, T. Narayanan, M. Sztuchi, P. Schall and G. H. Wegdam, Phys. Rev. Lett., 2008, **100**, 188303.
20 I. Jorjadze, L.-L. Pontani, K. A. Newhall and J. Brujić, PNAS, 2011, **108**, 4286–4291.
21 S. J. Veen, O. Antoniuk, B. Weber, M. A. Potenza, S. Mazzoni, P. Schall and G. H. Wegdam, Phys. Rev. Lett, 2012, **109**, 248302.
22 I. Jorjadze, L.-L. Pontani and J. Brujic, Phys. Rev. Lett., 2013, **110**, 048302.
23 H. Miki, T. Ishigami, J. Yamanaka, T. Okuzono, A. Toyotama, J. Mata, H. Komazawa, Y. Takeda, M. Minami, M. Fujita et al., npj Microgravity, 2023, **9**, 33.
24 T. E. Kodger, R. E. Guerra and J. Sprakel, Sci. Rep., 2015, **5**, 14635.
25 Y. Liu, T. Yanagishima, A. Curran, K. V. Edmond, S. Sacanna and R. P. Dullens, Langmuir, 2019, **35**, 7962–7969.
26 W. K. Kegel and A. van Blaaderen, Science, 2000, **287**, 290–293.
27 E. R. Weeks, J. C. Crocker, A. C. Levitt, A. Schofield and D. A. Weitz, Science, 2000, **287**, 627–631.
28 U. Gasser, E. R. Weeks, A. Schofield, P. Pusey and D. Weitz, Science, 2001, **292**, 258–262.
29 A. I. Campbell, V. J. Anderson, J. S. van Duijneveldt and P. Bartlett, Phys. Rev. Lett., 2005, **94**, 208301.
30 P. J. Lu, E. Zaccarelli, F. Ciulla, A. B. Schofield, F. Sciortino and D. A. Weitz, Nature, 2008, **453**, 499–503.
31 E. R. Russell, J. Sprakel, T. E. Kodger and D. A. Weitz, Soft Matter, 2012, **8**, 8697–8703.
32 H. Tsurusawa, J. Russo, M. Leocmach and H. Tanaka, Nat. Mater., 2017, **16**, 1022–1028.
33 J. Rouwhorst, C. Ness, S. Stoyanov, A. Zaccone and P. Schall, Nat. Commun., 2020, **11**, 3558.
34 H. Tsurusawa and H. Tanaka, Nat. Phys., 2023, 1–7.

35 J. Zhu, M. Li, R. Rogers, W. Meyer, R. Ottewill, S.-. S. S. Crew, W. Russel and P. Chaikin, Nature, 1997, **387**, 883–885.

36 A. Ikeda, L. Berthier and G. Biroli, J. Chem. Phys., 2013, **138**, 12A507.

37 S. Henkes, M. van Hecke and W. van Saarloos, Europhys. Lett., 2010, **90**, 14003.

38 Y. Wang, Y. Wang, X. Zheng, É. Ducrot, J. S. Yodh, M. Weck and D. J. Pine, Nat. Commun., 2015, **6**, 7253.

39 A. McMullen, M. Holmes-Cerfon, F. Sciortino, A. Y. Grosberg and J. Brujic, Phys. Rev. Lett., 2018, **121**, 138002.

40 A. McMullen, S. Hilgenfeldt and J. Brujic, PNAS, 2021, **118**, e2112604118.

41 A. McMullen, M. Muñoz Basagoiti, Z. Zeravcic and J. Brujic, Nature, 2022, **610**, 502–506.

42 M. Jerkins, M. Schröter, H. L. Swinney, T. J. Senden, M. Saadatfar and T. Aste, Phys. Rev. Lett., 2008, **101**, 018301.

43 P. Chaudhuri, L. Berthier and S. Sastry, Phys. Rev. Lett., 2010, **104**, 165701.

44 L. E. Silbert, Soft Matter, 2010, **6**, 2918–2924.

45 R. Seto, R. Mari, J. F. Morris and M. M. Denn, Phys. Rev. Lett., 2013, **111**, 218301.

46 H. Vinutha and S. Sastry, Nat. Phys., 2016, **12**, 578–583.

47 D. Vlassopoulos and M. Cloitre, Curr. Opin. Colloid Interf. Sci., 2014, **19**, 561–574.

48 R. P. Behringer and B. Chakraborty, Rep. Prog. Phys., 2018, **82**, 012601.

49 C. Zhang, N. Gnan, T. G. Mason, E. Zaccarelli and F. Scheffold, J. Stat. Mech. Theory Exp., 2016, **2016**, 094003.

50 B. J. Battersby, D. Bryant, W. Meutermans, D. Matthews, M. L. Smythe and M. Trau, J. Am. Chem. Soc., 2000, **122**, 2138–2139.

51 J. Dong, F. Turci, R. L. Jack, M. A. Faers and C. P. Royall, J. Chem. Phys., 2022, **156**, 214907.

52 Y. Wang, Y. Wang, D. R. Breed, V. N. Manoharan, L. Feng, A. D. Hollingsworth, M. Weck and D. J. Pine, Nature, 2012, **491**, 51–55.

53 Y. Zhang, A. McMullen, L.-L. Pontani, X. He, R. Sha, N. C. Seeman, J. Brujic and P. M. Chaikin, Nat. Commun., 2017, **8**, 21.

54 S.-H. Lee, Y. Roichman, G.-R. Yi, S.-H. Kim, S.-M. Yang, A. Van Blaaderen, P. Van Oostrum and D. G. Grier, Opt. Express, 2007, **15**, 18275–18282.

55 C. Martin, L. E. Altman, S. Rawat, A. Wang, D. G. Grier and V. N. Manoharan, Nat. Rev. Methods Primers, 2022, **2**, 83.

56 B. J. Krishnatreya, A. Colen-Landy, P. Hasebe, B. A. Bell, J. R. Jones, A. Sunda-Meya and D. G. Grier, Am. J. Phys., 2014, **82**, 23–31.

57 N. Chenouard, I. Smal, F. De Chaumont, M. Maška, I. F. Sbalzarini, Y. Gong, J. Cardinale, C. Carthel, S. Coraluppi, M. Winter et al., Nat. Methods, 2014, **11**, 281–289.

58 J. Schindelin, I. Arganda-Carreras, E. Frise, V. Kaynig, M. Longair, T. Pietzsch, S. Preibisch, C. Rueden, S. Saalfeld, B. Schmid et al., Nat. Methods, 2012, **9**, 676–682.

59 T. M. Obey and B. Vincent, J. Colloid. Interf. Sci., 1994, **163**, 454–463.

60 N. A. Elbers, J. Jose, A. Imhof and A. van Blaaderen, Chem. Mater., 2015, **27**, 1709–1719.

61 C. Van der Wel, G. L. Van de Stolpe, R. W. Verweij and D. J. Kraft, J. Phys. Condens. Matt., 2018, **30**, 094005.

62 K. Nagendra, A. Izzet, N. B. Judd, R. Zakine, L. Friedman, O. J. Harrison, L.-L. Pontani, L. Shapiro, B. Honig and J. Brujic, Biophys. J., 2023, **122**, 3506–3515.

63 L.-L. Pontani, M. F. Haase, I. Raczkowska and J. Brujic, Soft Matter, 2013, **9**, 7150–7157.

64 J. Lin, I. Jorjadze, L.-L. Pontani, M. Wyart and J. Brujic, Phys. Rev. Lett., 2016, **117**, 208001.

65 H. A. Makse, J. Brujic and S. F. Edwards, The Physics of Granular Media, 2004.

66 A. J. Liu and S. R. Nagel, Nature, 1998, **396**, 21–22.

67 E. DeGiuli, G. Düring, E. Lerner and M. Wyart, Phys. Rev. E, 2015, **91**, 062206.

68 E. DeGiuli, J. McElwaine and M. Wyart, Phys. Rev. E, 2016, **94**, 012904.

69 M. Trulsson, E. DeGiuli and M. Wyart, Phys. Rev. E, 2017, **95**, 012605.

70 B. Etcheverry, Y. Forterre and B. Metzger, Phys. Rev. X, 2023, **13**, 011024.

71 D. Z. Rocklin and X. Mao, Soft Matter, 2014, **10**, 7569–7576.

72 M. Ozawa, Y. Iwashita, W. Kob and F. Zamponi, Nat. Commun., 2023, **14**, 113.

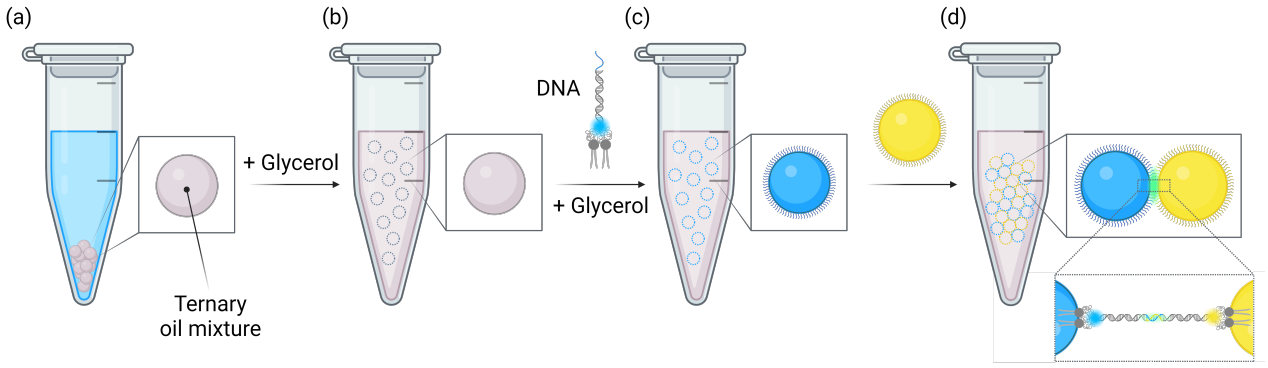

Fig. 1 Droplets of a ternary oil mixture (a) can be simultaneously density-matched and index-matched to a biocompatible glycerol solution (b). Matched droplets can be stabilized with lipid surfactants that also provide chemical functionality. Lipid-bound DNA strands, for example, endow droplets with specific affinity for other droplets displaying complementary DNA sequences (c). Multiple classes of DNA-functionalized droplets can be distinguished by fluorescent labeling and can be combined through split-and-mix processing to enable droplet-droplet assembly into clusters (d). These transparent, neutrally buoyant, programmable emulsions constitute an experimental toolbox for studying self-organization and the emergence of collective properties in complex multicomponent soft materials.

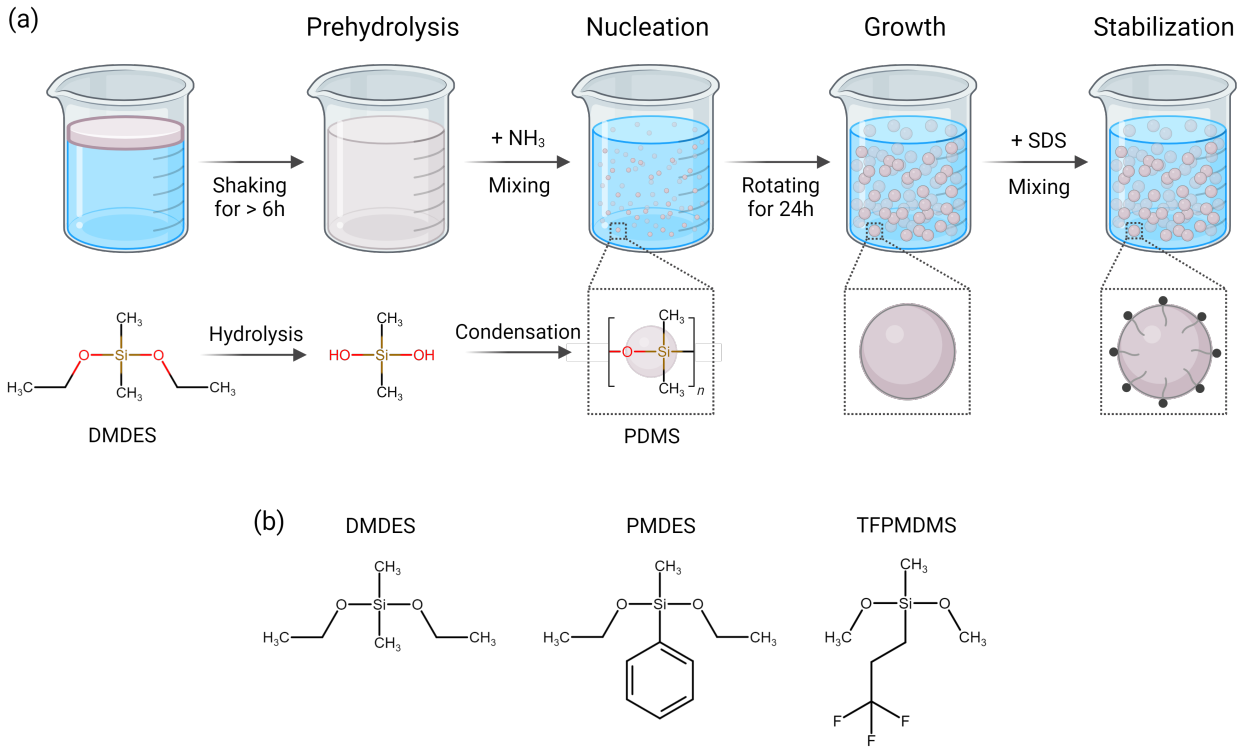

Fig. 2 (a) Schematic representation of the stages of droplet emulsification: prehydrolysis, nucleation, and growth. (b) Structural formulae of the three types of silane monomers used in the droplet formulation to achieve a wide range of densities and refractive indices.

Table 1 DNA sequences for functionalizing lipid-stabilized emulsion droplets. Complementary linker strands, L and L′, and palindromic strand, P, are listed from the 5′ end to the 3′ end. The complementary spacer strand, CS, is listed from 5′ to 3′. The L and L′ strands are fluorescently labeled with cyanine-5 and cyanine-3, respectively.

strand		3′	5′
L	azide Cy5	AGCAT TACTT TCCGT CCCGA GAGAC CTAAC TGACA CGCTT CCCAT CGCTA TTGTG AACTC TTGTG AACTC	
L′	azide Cy3	AGCAT TACTT TCCGT CCCGA GAGAC CTAAC TGACA CGCTT CCCAT CGCTA GAGTT CACAA GAGTT CACAA	
P	azide	AGCAT TACTT TCCGT CCCGA GAGAC CTAAC TGACA CGCTT CCCAT CGCTA TTTAT CGAT	
		5′	3′
CS	azide	TCGTA ATGAA AGGCA GGGCT CTCTG GATTG ACTGT GCGAA GGGTA GCGAT	

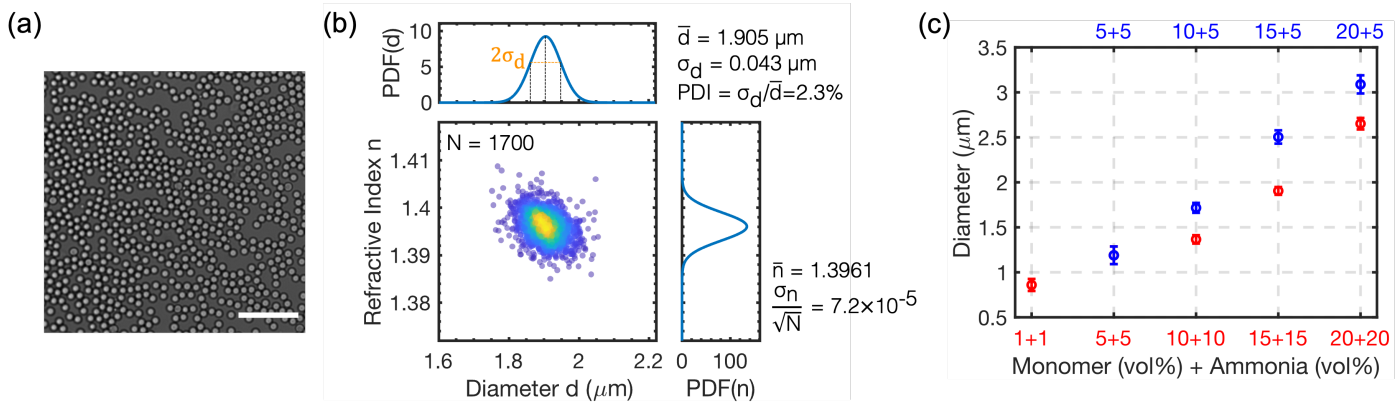

Fig. 3 (a) A typical microscopy image of monodisperse emulsion droplets. Scale bar is 50 μm. (b) Refractive index and diameter distribution measured by the XSight for a batch of droplets made using 15 vol% of both ammonia and DMDES monomer. Gaussian fits to the distributions give the Polydispersity index (PDI) of 2.3 % and the standard error of the refractive index (n) mean to the fifth decimal place. (c) Population-averaged droplet diameter increases as a function of DMDES monomer volume fraction at a fixed ratio (1:1) of monomer to ammonia (red) and as a function of their increasing volume fraction ratio (blue).

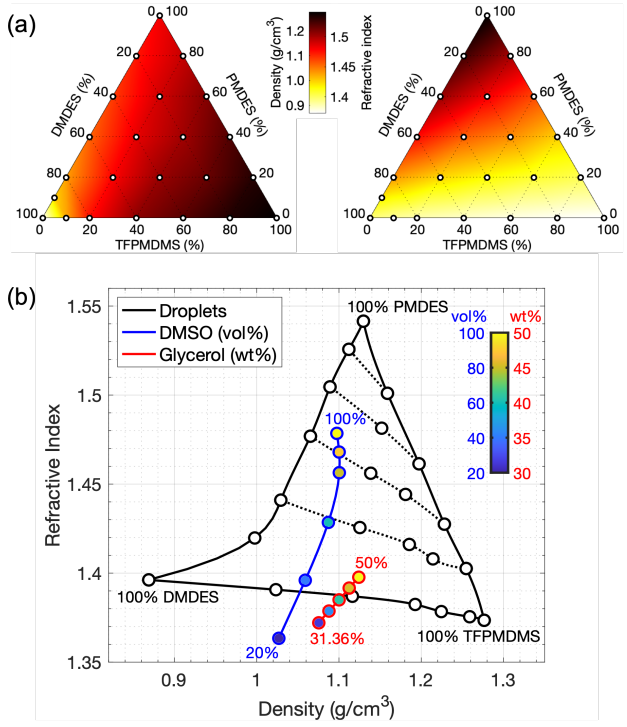

Fig. 4 (a) Ternary diagrams of the density (left) and the refractive index (right) of droplets that are synthesized using 5 vol% of ammonia and 5 vol% of monomers. Each circle represents a distinct droplet type made from a combination of the three distinct silane monomers: DMDES, PMDES, and TFPMDMS. (b) Plotting the refractive index as a function of the density for the data points in panel (a) reveals the matching aqueous phases with either DMSO (blue) or glycerol (red) in 1 mM SDS solution. Lines are interpolations between data points.

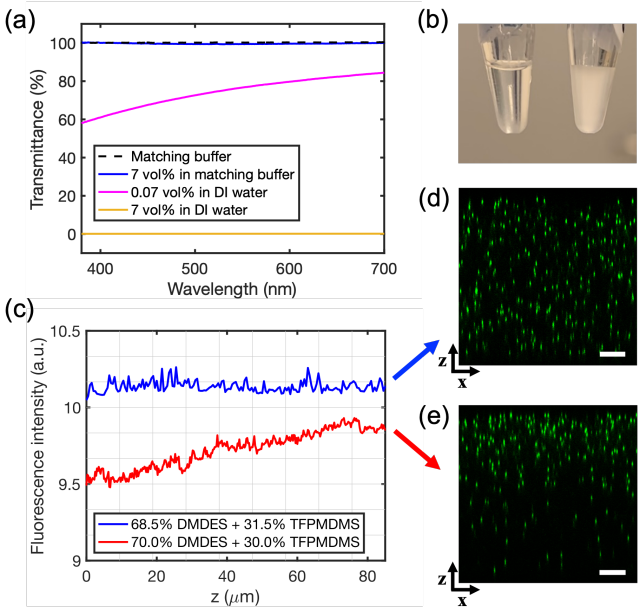

Fig. 5 Refractive index and density matching of droplets with a mean diameter of 1.5 μm. An optimally matched dispersion consists of droplets with a refractive index of 1.3861 ± 0.0002 (68.5 % DMDES, 31.5 % TFPMDMS) dispersed in a 41.6 wt% glycerol solution. UV-Vis transmittance (a) and visual inspection of macroscopic samples (b) show excellent transparency of the matched emulsion at 7.0 vol%, while the same emulsion in water shows no transmittance. (c) After a 5-day rest, confocal imaging of fluorescent droplets reveals a uniform vertical distribution for the matched emulsion (blue and (d)), and a linear upward trend for deliberately mismatched droplets (70.0 % DMDES and 30.0 % TFPMDMS, refractive index 1.3864 ± 0.0002, in a 41.9 wt% glycerol solution: red and (e)). Droplets are synthesized using 5 vol% monomers and 5 vol% ammonia. Scale bar: 20 μm.

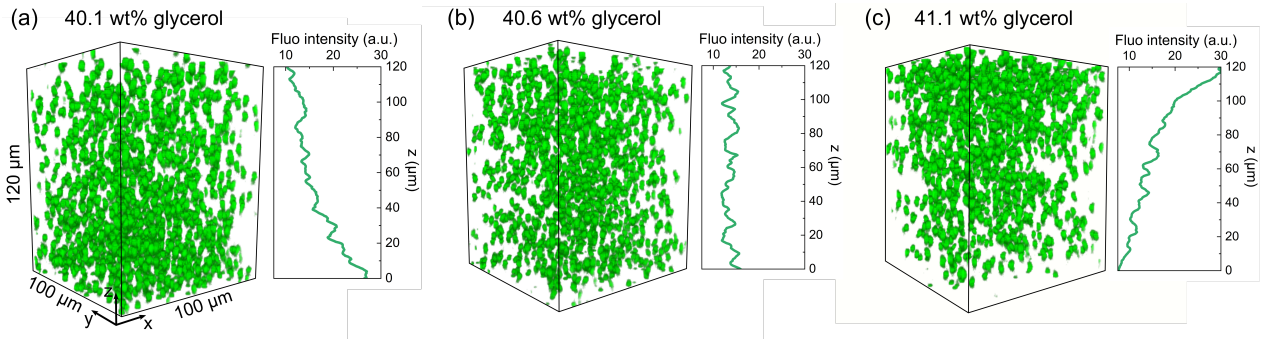

Fig. 6 Confocal microscopy images show that 3.5 µm-diameter transparent droplets either sink (a) or cream (c) after a 5-hour rest, but remain suspended (b) after a 30-min centrifugation at $100g$. The outcome is sensitive to the glycerol volume fraction to within 0.5 wt%, corresponding to a density difference of 0.001 g/cm^3. The emulsion consists of 4 vol% of droplets with a refractive index of 1.3850. The aqueous phase contains 5 mM SDS.

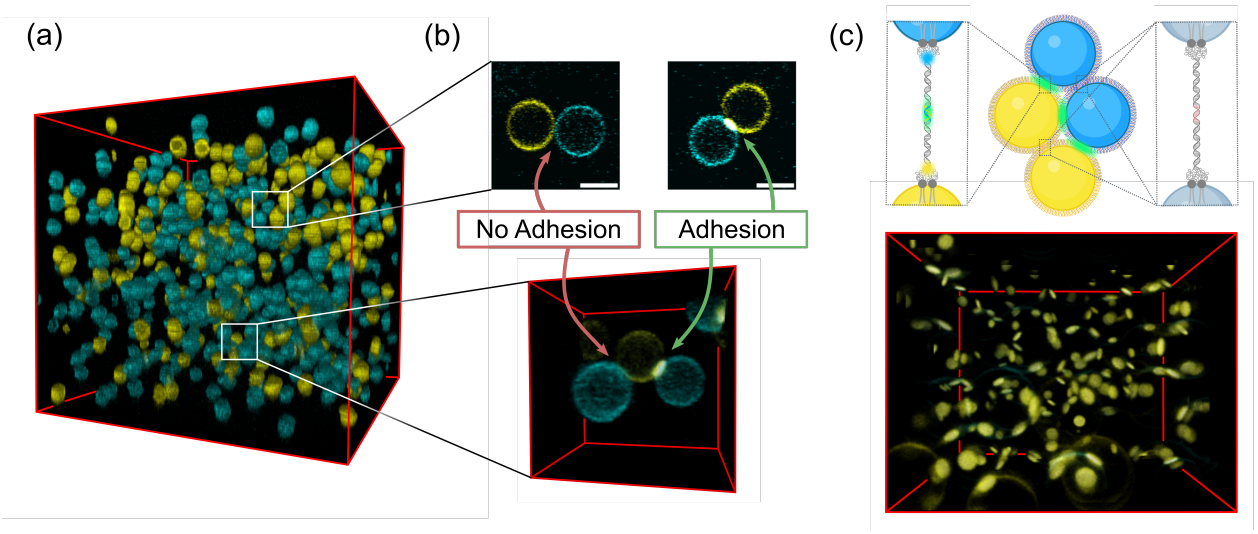

Fig. 7 Confocal images of DNA-functionalized droplets (6 µm diameter, refractive index 1.3850) in a matching aqueous solution containing 40.3 wt% glycerol. (a) 3D reconstruction of a mixture of 8 vol% droplets coated with complementary DNA (labeled in blue or yellow). Box size: 140 µm. (b) Zoomed-in images of representative dimers or trimers of droplets showing non-contacting or contacting droplets, as revealed by fluorescent adhesion patches formed through DNA hybridization. Scale bars: 5 µm. (c) Adding a palindromic DNA interaction between all droplets (shown in pink in the schematics) yields a highly interconnected colloidal gel. The transparency of the sample allows for a clear visualization of the distribution of $\sim$1.5 µm-diameter adhesion patches (bottom 3D projection). Box size: 30 µm.